

Mechanical, Magnetic, and Microstructural Characterization of $\text{Ni}_{0.9}\text{Co}_{0.1}\text{Fe}_2\text{O}_4$ Produced by the Ceramic Method

Mônica Sumie Hieda^a, João Paulo Barros Machado^b, Eduardo de Oliveira Silva Júnior^c, Mateus Botani de Souza Dias^d, Cristina Bormio Nunes^d, Rodrigo Gabas Amaro de Lima^a , Antonio Carlos da Cunha Migliano^{a,c}, Vera Lúcia Othéro de Brito^{a,c,*} 

^aPrograma de Pós Graduação em Ciências e Tecnologias Espaciais, Instituto Tecnológico de Aeronáutica, Praça Marechal Eduardo Gomes, 50, 12228-900, São José dos Campos, SP, Brasil
^bInstituto Nacional de Pesquisas Espaciais, Laboratório Associado de Sensores e Materiais, Avenida dos Astronautas, 1758, 12227-010, São José dos Campos, SP, Brasil
^cInstituto de Estudos Avançados, Trevo Coronel Aviador José Alberto Albano do Amarante, 1, 12228-001, São José dos Campos, SP, Brasil
^dEscola de Engenharia de Lorena, Universidade de São Paulo, Pólo Urbo-Industrial, Gleba AI-6, s/no., 12602-810, Lorena, SP, Brasil

Received: July 30, 2017; Revised: December 20, 2017; Accepted: January 18, 2018

Ni-Co ferrites, especially the ones with lower cobalt fractions, are candidate materials for applications in magnetomechanical sensors and electromagnetic wave absorbers. This work studied the microstructure, magnetostriction, flexural strength, and complex magnetic permeability of $\text{Ni}_{0.9}\text{Co}_{0.1}\text{Fe}_2\text{O}_4$, presenting data that weren't covered by previous literature on this composition. It was found that sieving the calcined powder before the forming operation increased the flexural strength of the ceramic. The Ni-Co ferrite had a saturation magnetostriction of 36ppm. The real part of the complex magnetic permeability varied between 2.2-2.3 in frequencies from 100MHz to 1GHz. In frequencies higher than 1GHz, μ' decreased sharply and reached 1 at 3.9GHz. It was found that the grinding media provided a small fraction of Al to the ferrite composition, which apparently affected the complex magnetic permeability of the material but the magnetostriction results were very close to Al-free Ni-Co ferrites with similar composition.

Keywords: ferrites, flexural strength, magnetostriction, complex magnetic permeability, magnetic ceramics.

1. Introduction

Ferrites are magnetic ceramics that have many applications in electronics, including magnetic^{1,2}, magnetoelectric³, and magnetomechanical sensors⁴. Among ferrites, the cobalt-based retains the highest magnetostriction levels, which makes them promising candidates for applications in magnetomechanical and magnetoelectric sensors^{5,6}. Ni-based ferrites also have interesting magnetostrictive properties for sensors applications^{7,8}. However, for some applications in magnetomechanical sensors, the material must have adequate mechanical strength, which requires strict control of the microstructure. The study of the mechanical properties of the ferrites is important not only for the development of ferrite magnetomechanical transducers but also for the development of surface-mounted devices (SMD) such as inductors and transformer cores⁹.

Ni-Co ferrites have spinel AB_2O_4 crystal structure, in which the oxygen anions are arranged in an FCC lattice and the Fe, Ni, and Co cations are distributed in one-eighth of

the tetrahedral (A) and one-half of the octahedral (B) and interstitial sites. The cation distribution in a spinel structure can be represented by (1), where D is a divalent cation, T is a trivalent cation, parentheses represent A sites, and brackets represent B sites¹⁰. The δ parameter is the degree of inversion, where $\delta=1$ for inverse spinels, $\delta=0$ for normal spinels, and $0<\delta<1$ for mixed spinels. The magnetic properties of the spinel ferrite depend on the cation distribution which, in turn, is affected by the processing parameters. For example, the cooling rate after sintering may affect the cation distribution. Ni-Co ferrites may be considered as a solid solution of CoFe_2O_4 in NiFe_2O_4 ¹¹, both inverse spinels¹⁰.



In NiFe_2O_4 , the substitution of Ni for Co tends to shift the magnetocrystalline anisotropy from negative to positive. In a certain Co fraction, the absolute anisotropy will thus reach a minimum, yielding a maximum in magnetic permeability¹¹.

*e-mail: vlobrito@ieav.cta.br

Chan et al.¹¹ found that, with $x=0.01$, the maximum magnetic permeability was attained in $\text{Ni}_{1-x}\text{Co}_x\text{Fe}_{1.98}\text{O}_4$, under the processing and sintering conditions used in their work.

Literature shows that the saturation magnetization (M_s) of $\text{Ni}_{1-x}\text{Co}_x\text{Fe}_2\text{O}_4$ increases with Co content⁷, varying from an average of 23 Am²/kg for $x=0$ to an average value of 57 Am²/kg for $x=1$ ^{7,12-16}. It is possible to observe a large dispersion of M_s values of Ni-Co ferrites with the same composition, but produced by different routes.

Chen et al.¹⁷ studied the electromagnetic properties of $\text{Ni}_{1-x}\text{Co}_x\text{Fe}_2\text{O}_4$ with $x=0.2, 0.5$, and 0.8 and found that these materials are good candidates for application as electromagnetic wave absorber in frequencies between 9-12GHz. The composition with $x=0.2$ had the best absorbing properties. The intrinsic electromagnetic absorption properties of a material are determined by its complex magnetic permeability and complex permittivity. The authors showed that both parameters of a Ni-Co ferrite increased when the Co content decreased.

Considering the potential applications of Ni-Co ferrites, especially the ones with low Co content, the aim of this work is to study the microstructure, magnetostriction, complex magnetic permeability, and flexural strength of $\text{Ni}_{0.9}\text{Co}_{0.1}\text{Fe}_2\text{O}_4$.

2. Experimental

The Ni-Co ferrite was produced by the ceramic method, with NiO, Fe₂O₃, and Co₃O₄ powders as raw materials. A laboratory ball mill, with alumina milling media, was used for mixing and milling. After wet mixing the raw materials with distilled water, the powder was dried and calcined at 900 °C for 4 h. The calcined material was then wet milled in the same mill and part of milled powder was sieved in a 125 μm sieve. The calcined powder was observed by scanning electron microscopy (SEM).

The powders were uniaxially compacted in round pellets of 8 mm diameter for microstructural examination and magnetostriction measurement. The samples for mechanical tests were uniaxially compacted with a 40MPa pressure, in the form of rectangular bars that had dimensions of 45 × 4.0 × 3.2 mm, approximately, after sintered at 1350 °C for 3h. The sample for complex permeability measurement was compacted in tube shape, with outer diameter of 8.32mm, inner diameter of 3.52mm and length of 15mm. The pellet and the tube compacts were sintered at 1350 °C for 3 h.

After sintering, the tube-shaped sample had length of 12mm, outer diameter of 6.8mm, and the inner diameter was machined to change from 2.9 to 3.1mm.

The ceramic samples in this work were identified as "AM" and "S", referring to the production from the as-milled and sieved calcined powder, respectively. The mechanical evaluation of the material was made by four-point bend tests, using an Instron Universal Test machine, model 1332. The number of tested specimens was 29 (AM) and 30 (S). Fig. 1 shows details of the experimental arrangement used in the test.

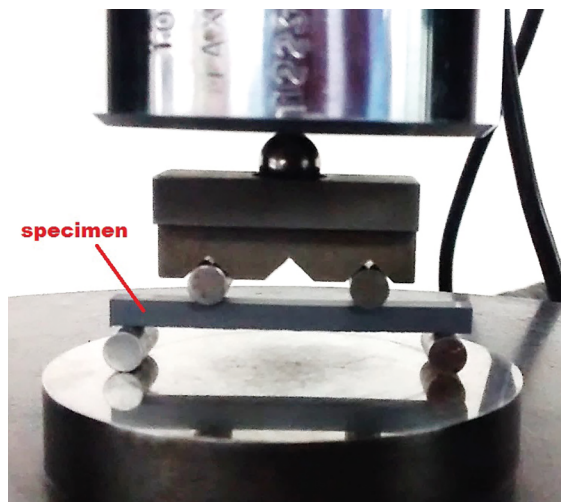


Figure 1. Picture of the experimental set-up of the bend test.

The crystal structures of the sintered pellets were analyzed by X-ray diffraction (XRD) analysis using Cu K α radiation. The lattice parameters (a) were calculated via Bragg's law¹⁸ and the Ni-Co ferrites density (d_{XRD}) was calculated from $d_{XRD} = \frac{SM}{Na^3}$, where M is the molecular weight of the ferrite and N is Avogadro's number. The densities (d) of such pellets were measured by the Archimedes' method and the relative density (D) was calculated as $(d/d_{XRD}) \times 100$.

The microstructure of the pellets and the fracture surfaces of the bend test specimens were evaluated by a SEM equipped with energy dispersive X-ray spectrometer (EDS). The grain size of the ferrite samples was measured by a linear intercept method, using images of the microstructure from a polished surface of the sintered pellets. The grain size measurement was made manually, with the aid of ImageJ software.

After mechanical evaluation, samples from the condition of higher strength (which were the ones produced from the sieved powder) underwent magnetic characterizations.

The magnetostriction (λ) measurements of the sintered ferrite pellet were carried out by the strain gauge method. λ represents the deformation of the material in a certain direction, as effect of a magnetic field ($\lambda = \Delta L/L_0$). A PA-06-060BG-350-LEN strain gauge from Excel Sensores was glued to the pellet with a LOCTITE 496 glue. Afterwards, the specimen was glued in a piece of cardboard and the cardboard assembly (Fig. 2) was placed in a support located between the poles of an EM4-HVA Lakeshore electromagnet. The change of the resistance of the strain gauge due to the magnetostrictive deformation was measured by a high speed Wheatstone bridge of National Instruments, model NI 9237, and the configuration used was 1/4 bridge, type I.

As represented in Fig. 3, the magnetostriction was measured in a direction parallel to the applied field (λ_{\parallel}) and perpendicular to the applied field (λ_{\perp}), after adjusting the position of the sample/strain gauge with respect to the applied field (parallel or perpendicular). The magnetic field was measured with a transversal Hall probe and a

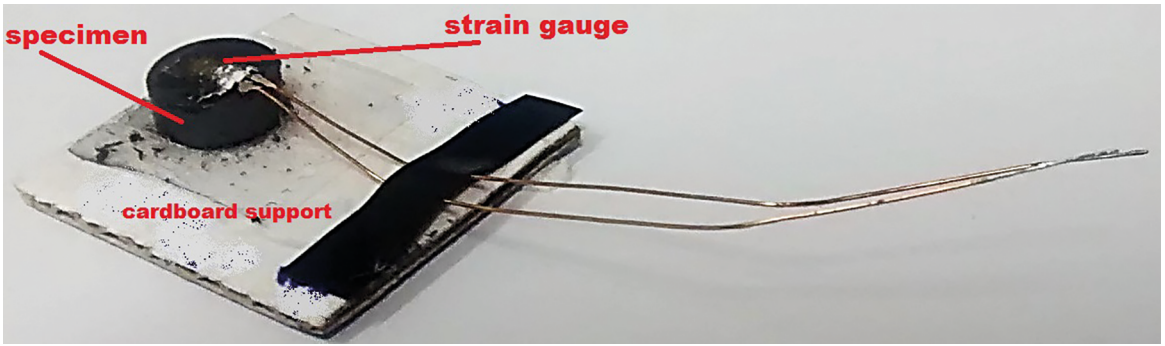


Figure 2. Cardboard assembly containing the pellet sample and strain gauge.

Gaussmeter model 452 from LakeShore, placed in the homogeneous region of the field. The magnetostriction data segments from $H=0$ to saturation were filtered with Origin[®] software, using the adjacent-averaging method and taking the moduli values of H and λ . The filtered segments were fitted with Origin[®] in Boltzmann functions, with adjusted $R^2=0.99918$ for the $\lambda_{//}$ curve and 0.99856 for the λ_{\perp} curve. The magnetoelastic sensitivities $S_{//}$ and S_{\perp} were calculated with Origin[®] by derivation of the fitted curves with respect to the applied field (H).

The complex magnetic permeability was measured using a vector network analyzer, Agilent PNA N5231A, which was calibrated for measurements in the 0.1-1GHz and 1-13.5 GHz frequency ranges. The sample holder utilized was an N-type coaxial air line (two-port device), suitable for samples with lengths up to 30.00 mm, 7.00 mm outer diameter and 3.04 mm inner diameter. The NRW algorithm^{19,20} was used in the PNA to calculate the complex magnetic permeability.

3. Results and Discussion

Figs. 4 and 5 show the SEM images of the sieved and as-milled calcined powders. From the micrographs it is possible to notice that the presence of large aggregates in the as-milled powder was eliminated with sieving. The sieved powder contains sub-micron particles.

Fig. 6 shows the diffraction patterns of the AM and S sintered pellets. Only peaks from the spinel phase were observed. The calculated lattice parameters were 8.284 \AA for the AM sample and 8.307 \AA for the S sample and the respective calculated d_{XRD} were 5.48 and 5.43 g/cm^3 . The difference in the lattice parameters indicates that the sieving operation may have influenced the chemical composition and, consequently, the value of the lattice parameter measured in the sintered pellets. Probably, it happened due to the occurrence of local chemical heterogeneities in the oxide mixture, which are very common in materials processed by the ceramic method. During calcination, this heterogeneity led to the formation of large aggregates with a chemical

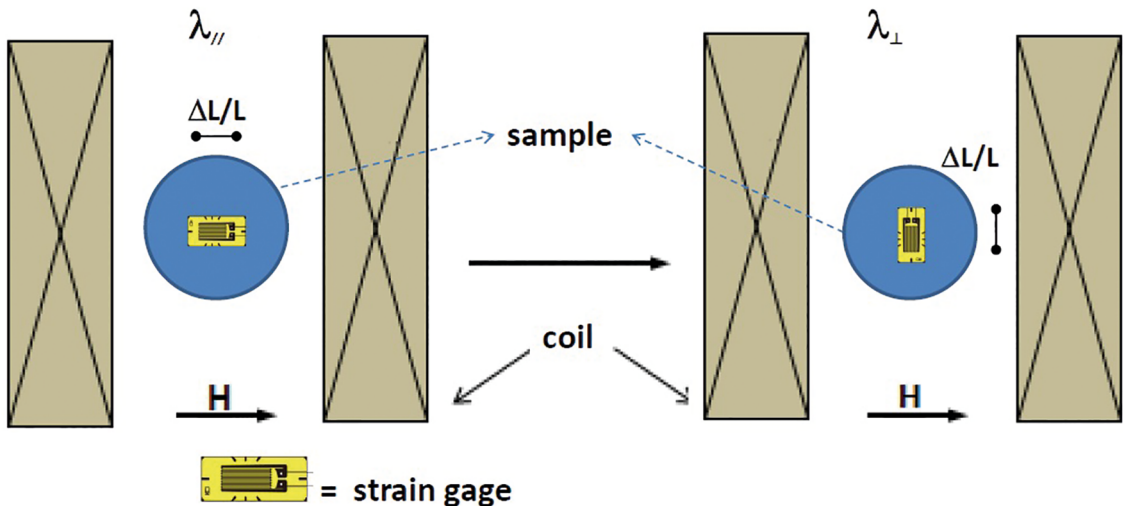


Figure 3. Scheme of the magnetostriction measurement method.

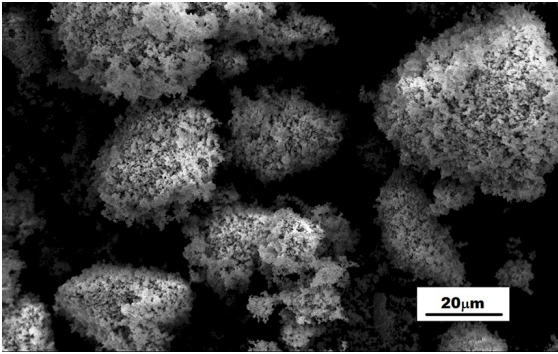


Figure 4. SEM image of the as-milled calcined powder.

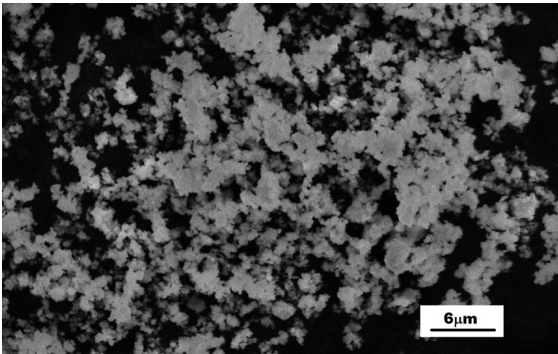


Figure 5. SEM image of the sieved calcined powder.

composition that was slightly different from the overall. The removal of these aggregates supposedly led to a small change in the composition of the sieved powder, thus affecting the value of the lattice parameter measured in the S sintered sample.

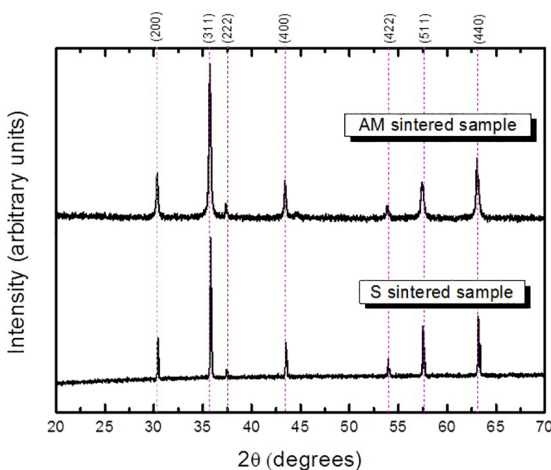


Figure 6. XRD patterns of the sintered ferrite pellets.

The measured densities of the AM and S pellets were 4.58 g/cm^3 ($D = 83.6\%$) and 4.70 g/cm^3 ($D = 86.5\%$), respectively. The closed porosity of the samples may be estimated as $100\% - D$, which means that the AM sample

is more porous. These results indicate that sieving caused the increase of the densification, caused by the removal of large aggregates.

The microstructures of the sintered ferrite pellets are shown on Figs. 7 and 8 and the results of the quantitative analysis are shown on Figs. 9 and 10. The S sample had slightly larger mean grain size and grain size distribution. The porosity of both samples was predominantly intergranular.

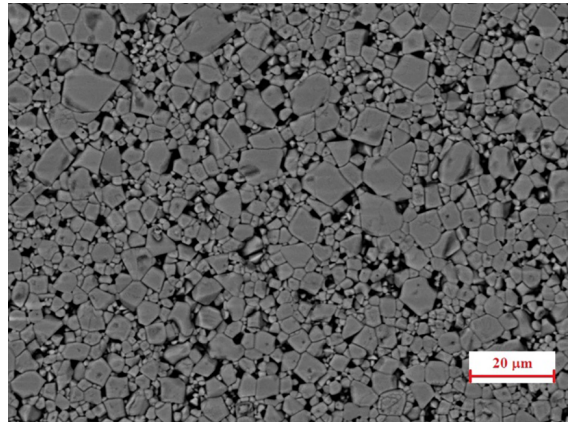


Figure 7. Microstructure of the sintered ferrite sample produced from the as-milled calcined powder.

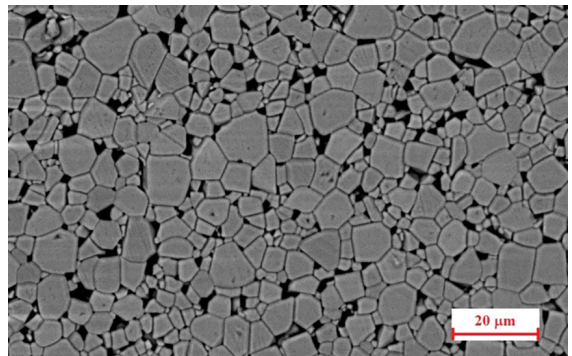


Figure 8. Microstructure of the sintered ferrite sample produced from the sieved calcined powder.

The porosity of a sintered ceramic is affected by the porosity of the green body. The porosity within the large agglomerates in the calcined powder will hardly be eliminated during compaction and this is why sieving may favor the attainment of greater green densities and sintered densities.

The results from the bend tests are represented in Fig. 11. In Tab. 1, the mean values, modes, and standard deviations are shown. The modes on Tab. 1 were defined after rounding the strength values to integers. From all specimens tested, the minimum strength reached was 35.6 MPa of AM sample and the maximum was 116 MPa of S sample. We didn't find data in literature for flexural strength of Ni-Co ferrite, but there are several works about mechanical strength of spinel ferrites. For comparison, the maximum strength obtained for a Ni-Zn ferrite doped with 5 wt% ZrO_2 was $\sim 110 \text{ MPa}$ and

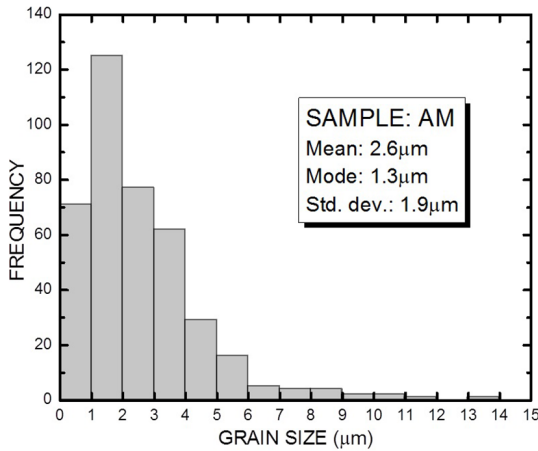


Figure 9. Grain size distribution of the AM sintered sample.

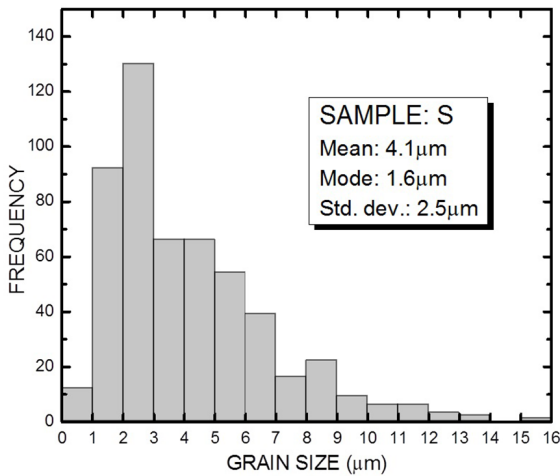


Figure 10. Grain size distribution of the S sintered sample.

the maximum strength of the bare ferrite was ~ 60 MPa in the work from Beseničar et al.²¹. Moreover, the strength of a Mn-Zn ferrite ranged from $\sim 60 - 110$ MPa, depending on the grain size and calcination temperature²² and a hot-isostatic pressed Ni-Zn ferrite presented 206 MPa²³.

It is well known that the mechanical strength of a ceramic is dependent on the quantity of defects in the sample, such as pores and cracks. So, to increase mechanical strength, the ceramic processing and sintering must be adjusted in order to obtain a dense and defect-free sample.

The presence of agglomerates and inhomogeneity in the compact leads to differential densification, which develops transient stresses during sintering. Following Rahaman et al.²⁴, these transient stresses may have the following effects in the compact during sintering: reduction in the densification rate in the surroundings of the agglomerates and inhomogeneities, cracking, and growth of pre-existing flaws. Therefore, the occurrence of more failures in stresses below 70 - 80 MPa in the AM samples, compared to the S samples may be related to the fact that AM samples have a more heterogeneous microstructure.

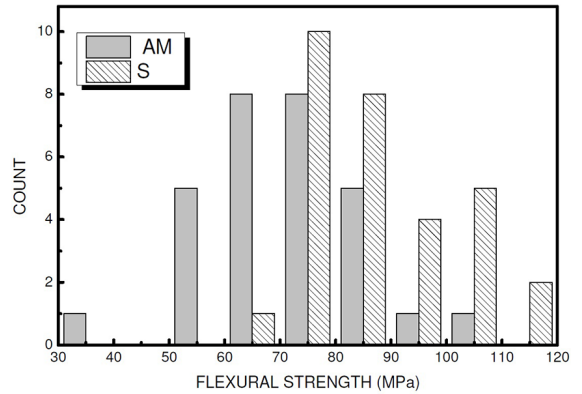


Figure 11. Histogram of the flexural strength measured in the bend tests.

Table 1. Flexural strength (MPa) of the AM and S sintered samples.

Mean	AM	S
Mode	70.4	86.9
St. Dev.	79	13.4

In order to increase the strength of a ceramic, it is necessary to increase its fracture toughness (K_{IC}) and to reduce the size of the largest crack in the ceramic body²⁵.

The S sample had higher mean flexural strength, but the microstructure of the samples from this batch (Fig.8) still presents a significant fraction of pores. The flexural strength improvement of the material through the reduction of the porosity may be achieved with the use of non-conventional sintering thermal cycles, such as the ones employed in two-step sintering, rate-controlled sintering, and fast-rate sintering²⁶⁻²⁸. In addition, isostatic pressing may also contribute to the increase of flexural strength, because it increases the green density, which favors densification during sintering.

Figs. 12-15 show the fracture surfaces of bend test specimens that presented flexural strengths near the calculated mean values presented in Tab. 1. A predominantly transgranular character of the fractures near the surfaces and intergranular or mixed character in the samples' center is evident. This finding suggests that the intergranular porosity is greater at the center of the samples. Indeed, the AM sample, which had the lowest flexural strength, presented intergranular fracture at the center (Fig. 12).

Having concluded that the sieving operation resulted in samples with higher density and less defects, the magnetic characterization was carried out in samples sintered from the sieved powder.

Fig. 16 shows the magnetostriction curves of the S sample. The saturation magnetostriction parallel to the field was -36ppm, which is higher than the value reported in²⁸ for a cobalt-free Ni ferrite ($\lambda_s = -26$ ppm for NiFe₂O₄) and very close to our previous result of -35ppm reported in ref.⁷ for an Al-free Ni-Co ferrite with similar composition. The magnitude of the saturation magnetostriction value of the NiCo ferrite is within the range from magnetostrictive

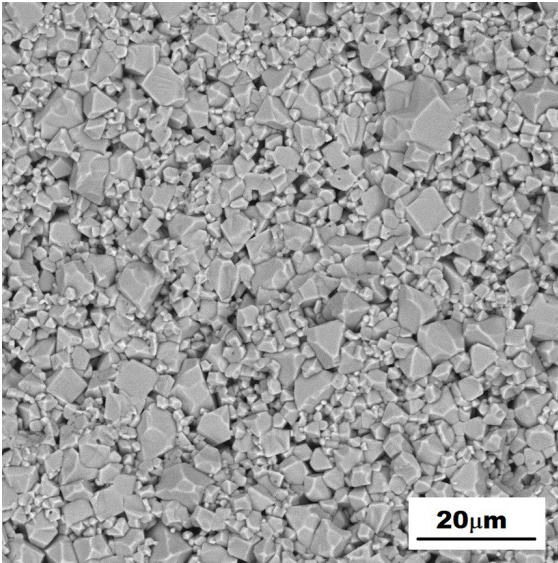


Figure 12. Fracture surface of an AM sample at the center, showing intergranular character.

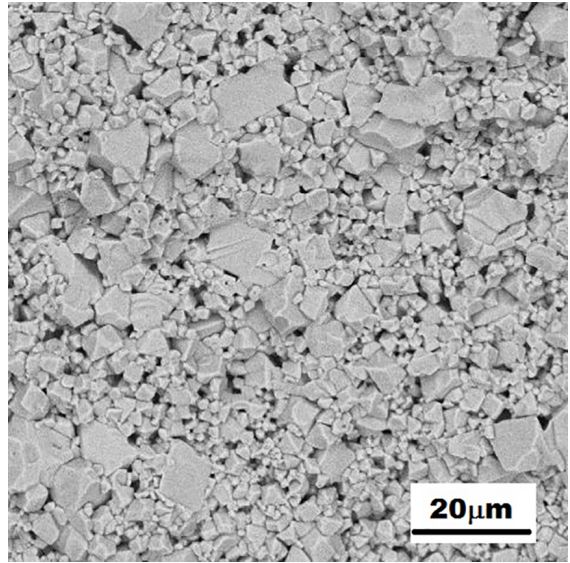


Figure 14. Fracture surface of an S sample at the center, showing mixed character (trans- and intergranular).

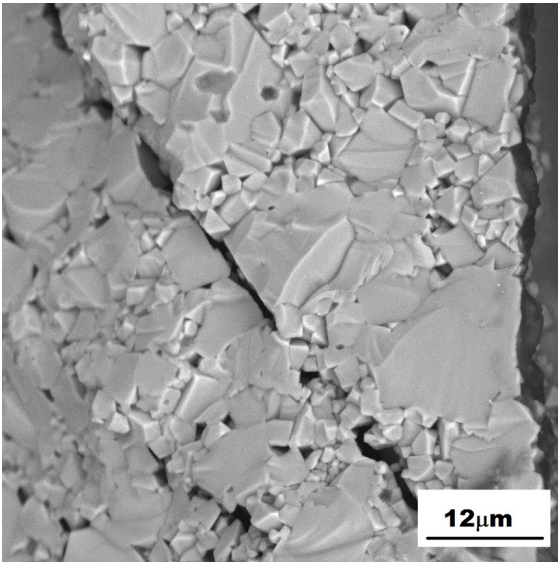


Figure 13. Fracture surface of an AM sample at the compression surface, showing a transgranular character.

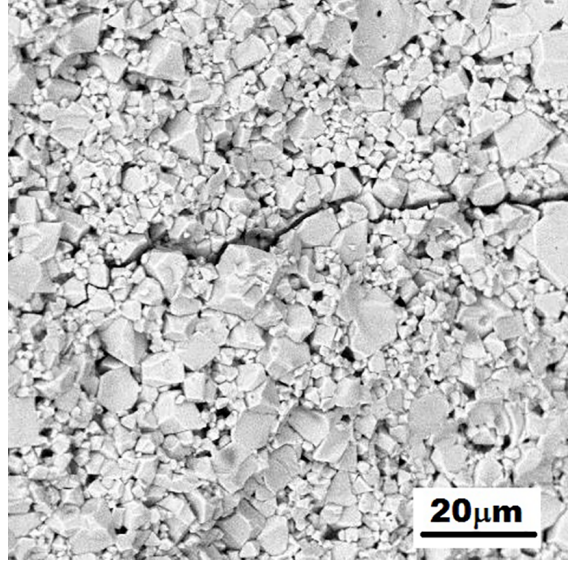


Figure 15. Fracture surface of an S sample at the compression surface, showing a redominantly transgranular character.

materials usually employed in sensors, such as amorphous iron alloys (30ppm, ref.²⁹).

For sensors applications, the magnetoelastic sensitivities $\frac{d\lambda}{dH}$ are in fact the relevant parameter for sensor project. Also, the magnetic field at which the maximum sensitivity occurs indicates the point of optimum performance of the material^{30,31}. The values of magnetoelastic sensitivity measured depend on the magnetic properties of the material and on the sample's geometry and dimensions⁶.

Fig. 17 shows the calculated magnetoelastic sensitivities of the sintered sample. Taking as reference the parameters measured parallel to the magnetic field, which are the more relevant for device applications, the maximum magnetoelastic sensitivity is 0.6×10^{-9} m/A, at 52 kA/m.

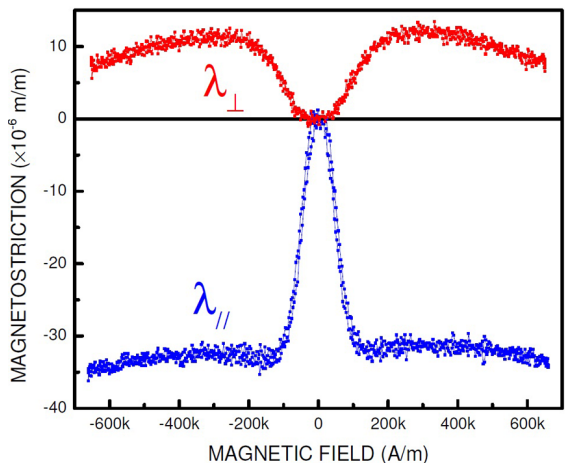


Figure 16. Magnetostriction curves of the sintered ferrite sample.

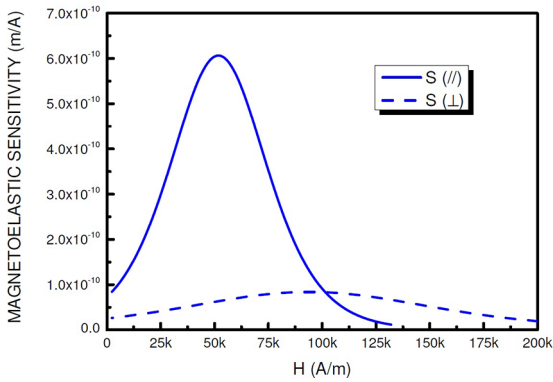


Figure 17. Moduli of magnetoelastic sensitivities of the sintered ferrite sample.

Figs. 18 and 19 show the complex magnetic permeability of the S sample. The real part (μ') is a function of the component of magnetization that is in phase with the AC magnetic field. The imaginary part (μ''), which relates to the magnetic losses, is a function of the component of the magnetization with a phase lag of 90° in relation to the field²⁹.

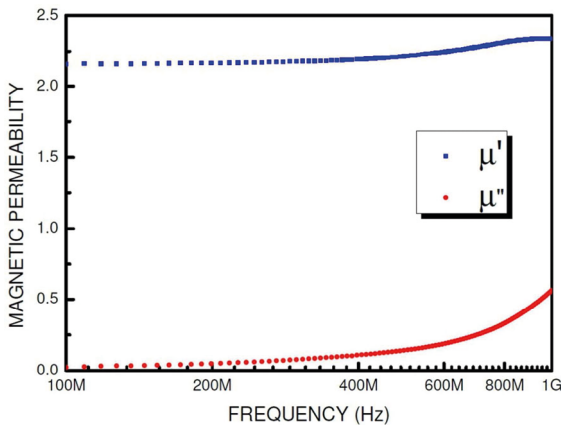


Figure 18. Complex magnetic permeability of the sintered ferrite sample, in frequencies between 100MHz-1GHz.

According to Figs. 18-19, μ' of the ferrite varied between 2.2-2.3 in frequencies from 100MHz to 1GHz. In frequencies higher than 1GHz, μ' decreased sharply and reached 1 at 3.9GHz. Xu³² measured the complex magnetic permeability of $\text{Ni}_{0.9}\text{Co}_{0.1}\text{Fe}_2\text{O}_4$, prepared by the citrate sol-gel technique, in frequencies below 1.5GHz and obtained μ' varying from 0.7-1.3.

The value of the magnetic permeability of a ferrite is highly dependent on the chemical composition, grain size, and porosity. Keeping the same processing conditions, grain size and porosity are determined by the sintering parameters. There are few data in literature for complex magnetic permeability

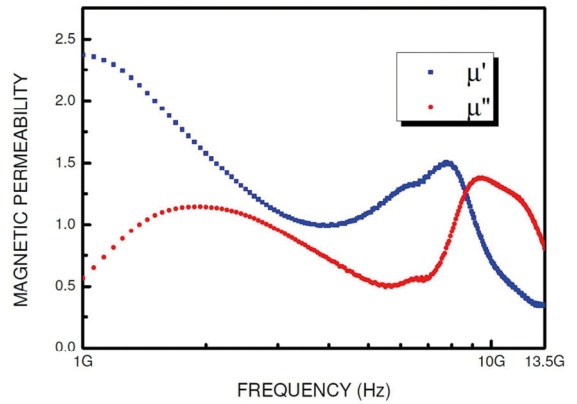


Figure 19. Complex magnetic permeability of the sintered ferrite sample, in frequencies between 1GHz-13.5GHz.

of $\text{Ni}_{0.9}\text{Co}_{0.1}\text{Fe}_2\text{O}_4$ but there are a lot of data for NiFe_2O_4 and some for NiCo ferrite with low Co fractions. Smit and Wijn³³ reported values of initial permeability ranging from 3 to 40 for NiFe_2O_4 with sintering temperature varying from 960 to 1450 °C, which resulted in porosity varying from 42% to 10%. The same authors, when studying the complex magnetic permeability of magnetic ceramics, reported a value of 10 for μ' of NiFe_2O_4 in frequencies from 0.1 to 100MHz. Chan et al.¹¹ reported $\mu'=15$ in a similar ferrite, in the same frequency range. The authors showed that μ' decreased to 10 adding Co in a fraction of 0.05 and increased to 22 with 0.01 Co fraction in $\text{Ni}_{1-x}\text{Co}_x\text{Fe}_{1.98}\text{O}_4$.

Chen et al.¹⁷ studied the electromagnetic properties of NiCo ferrites in frequencies from 2 to 18 GHz. In this frequency range, $\text{Ni}_{0.8}\text{Co}_{0.2}\text{Fe}_2\text{O}_4$ had a maximum μ' of 2.1 in a frequency near 3GHz, following a steep decrease until 6GHz. μ' reached 1 at 12GHz.

The μ' value at 100 MHz of the NiCo ferrite studied in this work was considerably lower than the values obtained by other authors for NiFe_2O_4 and $\text{Ni}_{1-x}\text{Co}_x\text{Fe}_2\text{O}_4$ with $x \leq 0.2$. However, in gigahertz frequencies, our results are closer to literature of those ferrite compositions.

In addition to factors such as difference in synthesis method, difference in porosity/grain size, and the presence of Co in the composition in a fraction of $x=0.1$, there is another factor that must be taken into consideration when comparing our complex permeability results to other from literature: EDS analysis (Fig. 20) detected the presence of Al in the ferrite, deriving from the alumina grinding media, and it certainly influenced the complex magnetic permeability results of our ferrite. Based on this analysis, the Al fraction in the sample was estimated as 1.12 wt%. It has been reported^{34,35} that the increase of the Al fraction in a Ni ferrite decreases the net magnetization because of the substitution of Fe^{3+} by Al^{3+} in the crystal lattice.

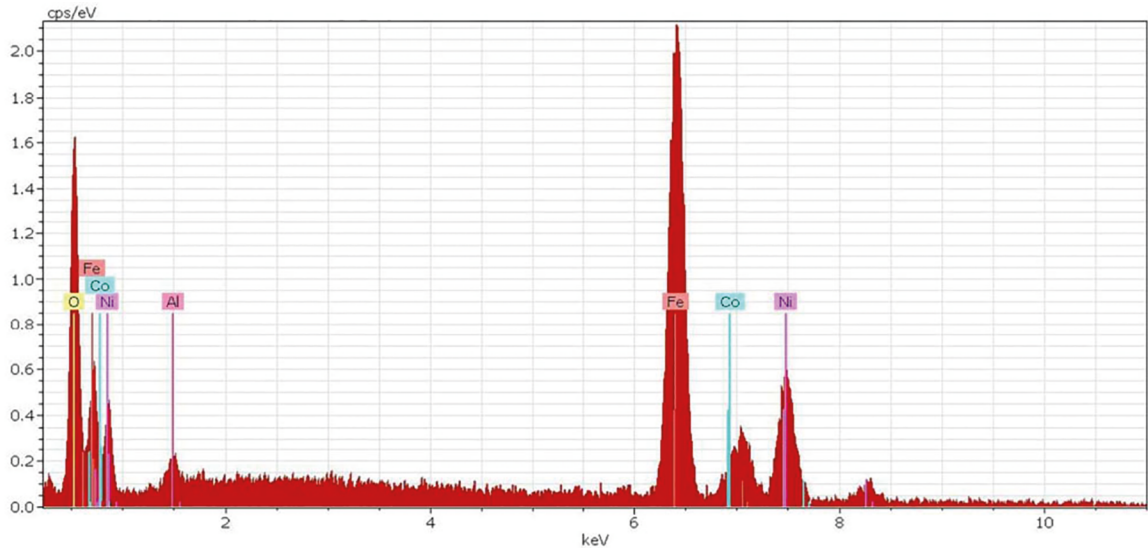


Figure 20. EDS spectrum of the sintered ferrite sample.

4. Conclusions

The results from this work indicate that sieving the calcined Ni-Co ferrite powder before the forming operation increased the flexural strength of the material. The use of alumina grinding media inserted Al in the ferrite composition and it apparently affected the magnetic permeability of the material, especially in the lowest frequencies studied. In spite of the Al content, the magnetostrictive properties of the ferrite were very close to other Al-free Ni-Co ferrites in literature with similar composition. The results also confirmed the potential applications of low-Co Ni-Co ferrites in sensors.

5. Acknowledgments

The authors acknowledge the support received from the following professionals and institutions:

- Materials Division of the Institute for Aeronautics and Space (São José dos Campos, Brazil), where the bend tests were made.
- Photonics Division of the Institute for Advanced Studies (São José dos Campos, Brazil).

This work has received financial support from CAPES (project no. 26 from Pró-Estratégia 2011 and scholarship from Instituto Tecnológico de Aeronáutica) and CNPq (grant no. 461334/2014-3).

6. References

1. Kim YH, Hashi S, Ishiyama K, Arai KI, Inoue M. Remote temperature sensing system using reverberated magnetic flux. *IEEE Transactions on Magnetics*. 2000;36(5):3643-3645.
2. Brito VLO, Migliano ACC, Lemos LV, Melo FCL. Ceramic processing route and characterization of a Ni-Zn ferrite for application in a pulsed-current monitor. *Progress in Electromagnetics Research*. 2009;91:303-318.
3. Bergs R, Islam RA, Vickers M, Stephanou H, Priya S. Magnetic field anomaly detector using magnetoelectric composites. *Journal of Applied Physics*. 2007;101(2):024108.
4. Stucki FF, inventor; Lockheed Corp., assignee. *Ferrimagnetic Pressure Transducer*. Great Britain patent GB 1.168.861. 1969 Oct 29.
5. Somaiah N, Jayaraman TV, Joy PA, Das D. Magnetic and magnetoelastic properties of Zn-doped cobalt-ferrites-CoFe₂Zn_xO₄ (x=0, 0.1, 0.2, and 0.3). *Journal of Magnetism and Magnetic Materials*. 2012;324(14):2286-2291.
6. Brito VLO, Cunha SA, Lemos LV, Nunes CB. Magnetic properties of liquid-phase sintered CoFe₂O₄ for application in magnetoelastic and magnetoelectric transducers. *Sensors (Basel)*. 2012;12(8):10086-10096.
7. Brito VLO, Cunha SA, Araújo FF, Machado JPB, Silva MR, Bormio-Nunes C. Processing and characterization of a Ni-Co ferrite for sensor applications. *Cerâmica*. 2015;61(359):341-349.
8. Sedlar M, Matejec V, Paulicka I. Optical fibre magnetic field sensors using ceramic magnetostrictive jackets. *Sensors and Actuators A: Physical*. 2000;84(3):297-302.
9. Choi HS, Kim KD, Jang JS. Design for reliability of ferrite for electronics materials. *Electronic Materials Letters*. 2011;7:63.
10. Valenzuela R. *Magnetic Ceramics*. Cambridge: Cambridge University Press; 1994.
11. Chan KC, Liew CT, Kong LB, Li ZW, Lin GQ. Ni_{1-x}Co_xFe_{1.98}O₄ Ferrite Ceramics with Promising Magneto-Dielectric Properties. *Journal of The American Ceramic Society*. 2008;91(12):3937-3942.
12. Khan K, Maqsood A, Anis-ur-Rehman A, Malik MA, Akram M. Structural, Dielectric and Magnetic Characterization of Nanocrystalline Ni-Co Ferrites. *Journal of Superconducting and Novel Magnetism*. 2012;25(8):2707-2711. DOI: 10.1007/s10948-011-1247-9

13. Mathe VL, Sheikh AD. Magnetostrictive properties of nanocrystalline Co-Ni ferrites. *Physica B: Condensed Matter*. 2010;405(17):3594-3598.
14. Xiang J, Chu Y, Shen X, Zhou G, Guo Y. Electrospinning preparation, characterization and magnetic properties of cobalt-nickel ferrite ($\text{Co}_{1-x}\text{Ni}_x\text{Fe}_2\text{O}_4$) nanofibers. *Journal of Colloid and Interface Science*. 2012;376(1):57-61.
15. Maaz K, Khalid W, Mumtaz A, Hasanain SK, Liu J, Duan JL. Magnetic characterization of $\text{Co}_{1-x}\text{Ni}_x\text{Fe}_2\text{O}_4$ ($0 \leq x \leq 1$) nanoparticles prepared by co-precipitation route. *Physica E: Low-dimensional Systems and Nanostructures*. 2009;41(4):593-599.
16. Niu ZP, Wang Y, Li FS. Magnetic properties of nanocrystalline Co-Ni ferrite. *Journal of Materials Science*. 2006;41:5726-5730.
17. Chen B, Chen D, Kang Z, Zhang Y. Preparation and microwave absorption properties of Ni-Co nanoferrites. *Journal of Alloys and Compounds*. 2015;618:222-226.
18. Callister WD Jr., Rethwisch DG. *Ciência e Engenharia de Materiais - Uma Introdução*. 9ª ed. Rio de Janeiro: LTC; 2016. 81 p.
19. Nicolson AM, Ross GF. Measurement of the Intrinsic Properties of Materials by Time-Domain Techniques. *IEEE Transactions on Instrumentation and Measurement*. 1970;19(4):377-382.
20. Weir WB. Automatic measurement of complex dielectric constant and permeability at microwave frequencies. *Proceedings of the IEEE*. 1974;62(1):33-36.
21. Beseničar S, Drogenik M, Kosmač T, Kraševc V. Magnetic and mechanical properties of ZrO_2 doped NiZn ferrites. *IEEE Transactions on Magnetics*. 1988;24(2):1838-1840.
22. Matsuo Y, Ono K, Hashimoto T, Nakao F. Magnetic properties and mechanical strength of MnZn ferrite. *IEEE Transactions on Magnetics*. 2001;37(4):2369-2372.
23. Yang Z, Xiao-Ping B. The effect of post-heat treatment on structure, magnetic and mechanical properties of hot isostatic pressed (HIP) NiZn ferrite. *IEEE Transactions on Magnetics*. 1989;25(5):4239-4241.
24. Rahaman MN. *Ceramic Processing and Sintering*. 2nd ed. Boca Raton: CRC Press; 2003.
25. Wachtman JB. *Mechanical Properties of Ceramics*. 1st ed. New York: John Wiley & Sons; 1996.
26. Rafferty A, Prescott T, Brabazon D. Sintering behaviour of cobalt ferrite ceramic. *Ceramics International*. 2008;34(1):15-21.
27. Zhang Z, Liu Y, Yao G, Zu G, Wu D, Hao Y. Synthesis and characterization of dense and fine nickel ferrite ceramics through two-step sintering. *Ceramics International*. 2012;38(4):3343-3350.
28. Wang XH, Deng XY, Bai HL, Zhou H, Qu WG, Li LT, et al. Two-Step Sintering of Ceramics with Constant Grain-Size, II: BaTiO₃ and Ni-Cu-Zn Ferrite. *Journal of the American Ceramic Society*. 2006;89(2):438-443.
29. du Trémolet de Lacheisserie E, Gignoux D, Schlenker M, eds. *Magnetism, Materials & Applications*. New York: Springer; 2005.
30. Lu C, Xu C, Wang L, Gao J, Gui J, Lin C. Investigation of optimized end-bonding magnetoelectric heterostructure for sensitive magnetic field sensor. *Review of Scientific Instruments*. 2014;85(11):115003.
31. Srinivasan G, Hayes R, DeVreugd CP, Laletsin VM, Paddubnaya N. Dynamic magnetoelectric effects in bulk and layered composites of cobalt zinc ferrite and lead zirconate titanate. *Applied Physics A*. 2005;80(4):891-897.
32. Xu C. Magnetic and Microwave Absorption Properties of $\text{Ni}_{1-x}\text{Co}_x\text{Fe}_2\text{O}_4$ Nanometer Powders in GHz Frequencies. *Materials Science Forum*. 2011;694:380-384.
33. Smit J, Wijn HPJ. *Ferrites: Physical properties of ferromagnetic oxides in relation to their technical applications*. Eindhoven: Philips Research Laboratories; 1959. p. 169, 269.
34. Bhosale AG, Chougule BK. X-ray, infrared and magnetic studies of Al-substituted Ni ferrites. *Materials Chemistry and Physics*. 2006;97(2-3):273-276.
35. Raghavender AT, Pajic D, Zadro K, Milekovic T, Venkateshwar Rao P, Jadhav KM, et al. Synthesis and magnetic properties of $\text{NiFe}_{2-x}\text{Al}_x\text{O}_4$ nanoparticles. *Journal of Magnetism and Magnetic Materials*. 2007;316(1):1-7.